Optical design and characterization of an advanced computational imaging system

Optical Design and Characterization of an Advanced Computational Imaging System

R. Hamilton Shepard[1*], Christy Fernandez-Cull[1], Ramesh Raskar[2], Boxin Shi[2,3], Christopher Barsi[2], and Hang Zhao[2]
[1]Lincoln Laboratory, Massachusetts Institute of Technology, 244 Wood Street, Lexington, MA, 02420
[2]MIT Media Lab, Massachusetts Institute of Technology, 75 Amherst Street, Cambridge, MA, 02139
[3]Singapore University of Technology and Design, 20 Dover Dr., Singapore, 138682

ABSTRACT

We describe an advanced computational imaging system with an optical architecture that enables simultaneous and dynamic pupil-plane and image-plane coding accommodating several task-specific applications. We assess the optical requirement trades associated with custom and commercial-off-the-shelf (COTS) optics and converge on the development of two low-cost and robust COTS testbeds. The first is a coded-aperture programmable pixel imager employing a digital micromirror device (DMD) for image plane per-pixel oversampling and spatial super-resolution experiments. The second is a simultaneous pupil-encoded and time-encoded imager employing a DMD for pupil apodization or a deformable mirror for wavefront coding experiments. These two testbeds are built to leverage two MIT Lincoln Laboratory focal plane arrays – an orthogonal transfer CCD with non-uniform pixel sampling and on-chip dithering and a digital readout integrated circuit (DROIC) with advanced on-chip per-pixel processing capabilities. This paper discusses the derivation of optical component requirements, optical design metrics, and performance analyses for the two testbeds built.
Keywords: coded aperture imaging, super-resolution, computational imaging, compressive sensing, smart processing, multiplexing, pupil coding, point spread function engineering

1. INTRODUCTION

Multi-modal imaging platforms for task-specific sensing have been developed conceptually and signal recovery performance analysis has been studied. These address object-plane coding, spatial-spectral encoding, pupil-plane coding, and pixel-coding schemes.[1-7] Much of the extensive body of literature addressing optical encoding with static apertures arises from the fields of coded-aperture imaging, computational imaging, and more recently compressive sensing. Challenges associated with existing approaches include static apertures that suffer from diffraction effects, signal-to-noise ratio penalties associated with aperture opacity, lack of measurement diversity, and aperture-code to pixel registration issues. Dynamic apertures for image- and pupil-plane encoding improve upon measurement diversity and signal recovery when using compressive sensing algorithms.[8-9] In an attempt to leverage benefits associated with dynamic apertures, some flexible optical architectures providing simultaneous access to intermediate image and pupil planes exist in the literature but focus on spatial-spectral and light-field imaging for computational photography.[2] We have developed an advanced computational imaging system (ACIS) concept to provide a flexible optical architecture for spatial-spectral (x,y,λ), spatial-temporal (x,y,t), and spatial-depth (x,y,z) imaging experiments via simultaneous and dynamic object encoding at image and pupil planes.

The ACIS concept manifests itself as two testbeds. The first is a coded-aperture programmable pixel imager (CAPPI) that employs a similar optical architecture to the Rice single-pixel camera where a high-resolution digital micromirror device (DMD) is used to encode object data onto a single pixel.[10-11] We differ from the Rice single-pixel camera in our illumination design for a spatially extended scene and image encoding tactics where target data is imaged onto a two-

*Hamilton.Shepard@ll.mit.edu

This work is sponsored by the Assistant Secretary of Defense for Research and Engineering under Air Force contract #FA8721-05-C-002. Opinions interpretations, conclusions and recommendations are those of the authors and are not necessarily endorsed by the United States Government.

Optics and Photonics for Information Processing VIII, edited by Abdul A. S. Awwal, Khan M. Iftekharuddin, Mohammad A. Matin, Andrés Márquez, Proc. of SPIE Vol. 9216, 92160A © 2014 SPIE
CCC code: 0277-786X/14/$18 · doi: 10.1117/12.2060725

dimensional (2D) detector array of pixels instead of a single pixel. Thus, every pixel is oversampled by a maximum factor of thirty-six at diffraction-limited performance. Implications associated with this testbed pertain ideally to infrared wavelengths where the pixel pitch is large (i.e., 15-30 μm) and detector resolution is still less than 2MP. Our testbed combined with compressive sensing algorithms shows promise to extend sub-megapixel class imagers to tens of megapixels or more.

The second testbed is a dynamic pupil-encoding and time-encoding imager (PETEI) that allows simultaneous pupil- and image-plane coding. This testbed employs a DMD for pupil apodization and a deformable mirror (DM) for wavefront coding experiments. Time-encoding results from aperture modulation synchronization with the readout rate of an MIT Lincoln Laboratory (MIT LL) focal plane array. Also, a per-pixel flutter shutter operation at the focal plane array enables a time-coded modulation that requires no mechanical translation of an aperture placed at the pixel. Prior-art shows temporal multiplexing using structured illumination and mechanical aperture-code translation for high-speed and high-resolution imaging, spatial super-resolution, and extended depth of focus imaging.[12-17] We have previously shown the utility of MIT LL focal plane arrays for high-speed transient imaging of hyper-temporal targets by leveraging in-pixel flutter shutter capabilities combined with on-chip processing.[18-20] Our PETEI testbed combines dynamic optical encoding at the pupil plane with novel focal plane array on-chip and per-pixel flutter shutter to realize image plane coding with no mechanical moving parts. PETEI is used to realize applications such as passive 3D ranging, pixel super-resolution, and extended depth of focus with the addition of a compressive sensing framework. The authors have recently presented the PETEI concept elsewhere.[21] This paper focuses on the optical design and hardware implementation of the testbeds.

The ACIS testbeds, CAPPI and PETEI, leverage MIT LL focal plane arrays re-purposed as computational imaging arrays (CIAs). The orthogonal transfer (OT) CCD employs a unique non-uniform pixel architecture that has been shown in simulation and with preliminary experiments to overcome the pixel sample rate with additional processing post data capture.[22] We leverage the OT pixel asymmetry as a 4-phase device as well as OT on-chip phase shifting capabilities previously used for motion compensation in ground-based astronomy applications.[23-24] The PETEI ACIS testbed draws upon previous work for on-chip coded-aperture temporal imaging utilizing a digital readout integrated circuit (DROIC) with a per-pixel shutter for temporal super-resolution. [19] A major advantage associated with dynamic digital in-pixel shuttering includes flux preservation when a time-varying binary (1,-1) aperture is utilized versus typically used static apertures placed along the optical axis. Finally, DROIC pixel processing imagers (PPIs) re-purposed as CIAs provide in-pixel analog-to-digital conversion and per-pixel processing allowing for novel spatial and temporal filtering and dynamic range enhancements as compared to conventional 2D focal plane arrays.[25-27]

Development of CAPPI and PETEI to achieve ACIS objectives involves satisfying multiple requirements related to image quality, data sampling, radiometry, and packaging considerations. In this paper, we focus on the optical design, development, and characterization of the testbeds. We discuss design considerations, performance trades, alignment challenges as well as explain how the initial ACIS concept manifested itself into two low-cost and robust commercial-off-the-shelf (COTS) testbeds meant to address the ACIS objective – flexible, simultaneous, and dynamic object plane integer and integer-multiple sampling and pupil-plane coding .

This paper is organized as follows. Section 2 provides an overview of the process of selecting COTS optical components for testbed development and the implications associated with using the components in configurations that did not motivate the original design. Considerations include details such as vignetting in a relay constructed from lenses without proper pupil or numerical aperture matching, and how shifting the aperture stop of a lens to a spatial light modulator (SLM), for pupil encoding, affects lens aberrations. Finally, we provide an overview of an ideal imaging testbed that satisfies both object and pupil coding. Evaluation of the testbed requirements led to a conclusion that custom optical components would be required. We, instead, designed two low-cost and flexible COTS testbeds to meet the ACIS goal. In Section 3, we describe the design and characterization of an object-plane coding testbed – CAPPI . Section 4 discusses the design and hardware associated with a pupil-plane coding testbed (PETEI) that when combined with simultaneous dynamic on-chip capabilities produces the effect of the ideal testbed without the use of custom optics. Finally, in Section 5, we summarize our testbed developments and foreshadow future work.

2. ADVANCED COMPUTATIONAL IMAGING SYSTEM DESIGN TRADES

The advanced computational imaging system (ACIS) addresses the need for a flexible optical architecture accommodating object oversampling via image plane coding, object integer sampling for space-time encoding at the pixel resolution, and pupil encoding for novel point spread function engineering. Pupil coding or wavefront coding for point spread function engineering has shown promise for enhanced pixel-based spatial super-resolution and depth-of-field enhancement.[28-31] When combined with a dynamic time-varying and time-synchronized spatial or temporal object encoding, an advanced computational imaging system is obtained. A flexible optical architecture that enables simultaneous and dynamic pupil- and image-plane encoding enables pixel-based super-resolution, depth super-resolution, and temporal-super resolution imaging. This section evaluates the requirements associated with a notional testbed that achieves the ACIS goal.

Dynamic pupil encoding is possible through the use of any number of spatial light modulator technologies such as a DMD or liquid crystal array for amplitude coding, or a deformable mirror for wavefront coding. For uniform encoding across the entire field of view (FOV), the encoding device must be placed at the aperture stop location or in any conjugate pupil plane. Another consideration is the encoder response as a function of field angle, which may limit the FOV of the system depending on the SLM technology. An ideal optical system for dynamic pupil coding would be designed with an external aperture stop at which to place the SLM. As the stop position deviates from the design value, the well known effects of stop shifting[31] modify the aberrations of the optical system and may impose a restriction to the system F/# and FOV to reduce vignetting. An example of these effects is shown in Section 4.

Object or image plane encoding can be accomplished in a number of ways. Binary or grayscale masking of the object may be introduced at the object itself or at any conjugate image plane. In the mathematical representation, these options are functionally equivalent; however, they introduce important tradeoffs related to the optical system architecture.

The object may be encoded directly via structured illumination. Both contrast and resolution become more challenging with increased object distance by placing demands on the transmitted power, aperture size, and image quality of the projection system. Alternatively, the encoding mechanism may be applied directly to the image plane or any conjugate intermediate focus location. Image coding at the sensor's focal plane is convenient as it minimally impacts the optical design requirements, yet this may be impossible given the limitations of most commercially available cameras (e.g. stationary non-reconfigurable pixels with limited temporal sampling flexibility).

An intermediate image plane is a desirable location to place an SLM such as a digital micromirror device (DMD), or a mechanical or LCD shutter array. With this arrangement the image plane is directly accessible without interfering with the camera design or packaging. Additionally, magnification may be used between the intermediate and final image planes to obtain the desired encoding resolution when constrained with fixed pixel or encoding element sizes. However, while an intermediate image presents a flexible location to place the SLM, it also has the most impact on the optical design. To create an intermediate image an objective lens is used to create a prime focus which is subsequently reimaged to the camera using a relay lens group. Both sub-systems must have a sufficient working distance to accommodate the encoding element and their pupils must be matched to minimize vignetting over the FOV. Minimizing the range of incident angles across the intermediate image may also be required if the SLM has an angularly dependant response. Such may be the case with an LCD array that has variable transmission vs. viewing angle, or with a DMD that has a maximum acceptance angle to separate the input and output beam paths. A telecentric optical design can be used to improve the uniformity of incident ray angles at the image.

In a telecentric optical design the chief ray from every field point comes to focus parallel to the optical axis, or stated another way, the focusing cone of light is normal to the image surface across the entire FOV. This is achieved by placing the aperture stop (or any conjugate pupil image location) at the front focal point of the optical system. An intermediate image formed between two telecentric optical systems of the same F/# provides pupil matching and uniform incident angles across the focal surface as shown in Figure 1. A telecentric optical design also provides the opportunity for an external aperture stop at which to place a pupil encoding SLM, which is a convenient optical layout to realize the pupil encoding goal of ACIS.

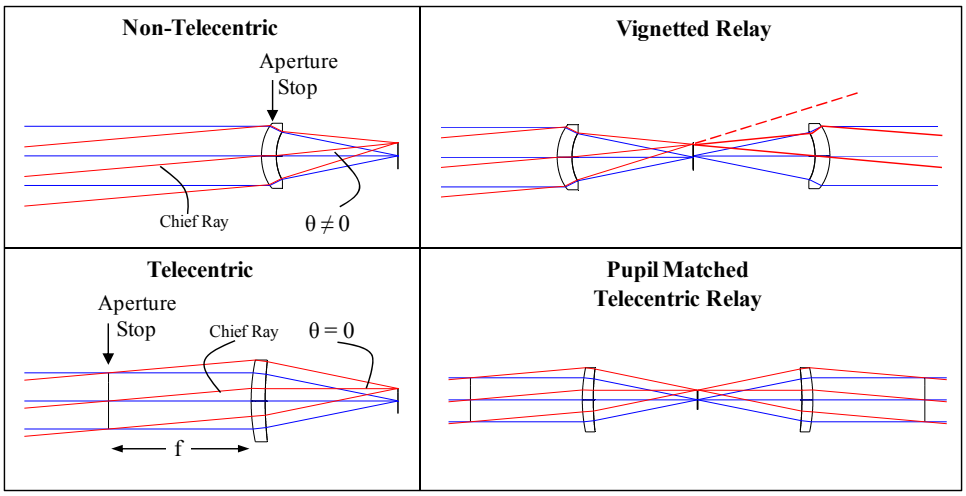

Figure 1. Image plane incident angles and pupil matching in telecentric and non-telecentric relays. Telecentric lenses operating at the same F/# are naturally pupil matched.

A notional design for a flexible computational imaging testbed that allows for both pupil and intermediate image plane coding is shown in Figure 2. The design is constructed from three individually aberration corrected infinite-conjugate telecentric lens groups with external pupils. If 1:1 magnification between the intermediate and final images is permitted, this design strategy allows for a single optical sub-assembly to be designed and then repeated three times in sequence to create a computational imaging testbed. Finite-conjugate telecentric lenses are commercially available from multiple suppliers; however infinite-conjugate telecentric lenses likely require a custom design. Correcting certain aberrations including coma, distortion, and lateral color is challenging in this layout because the individual systems lack symmetry for aberration balancing, and by cascading 3 lenses the aberrations sum. In Figure 2, the layout is shown with the intermediate image plane used in transmission corresponding to usage with a transmissive shutter array for image encoding. The secondary pupil image is a result of the telecentric layout and could be used with an iris to control the system F/# or pupil size at the SLM. If a reflective encoding element such as a DMD is desired the working distance could be increased to accommodate a beam splitter in the intermediate image space.

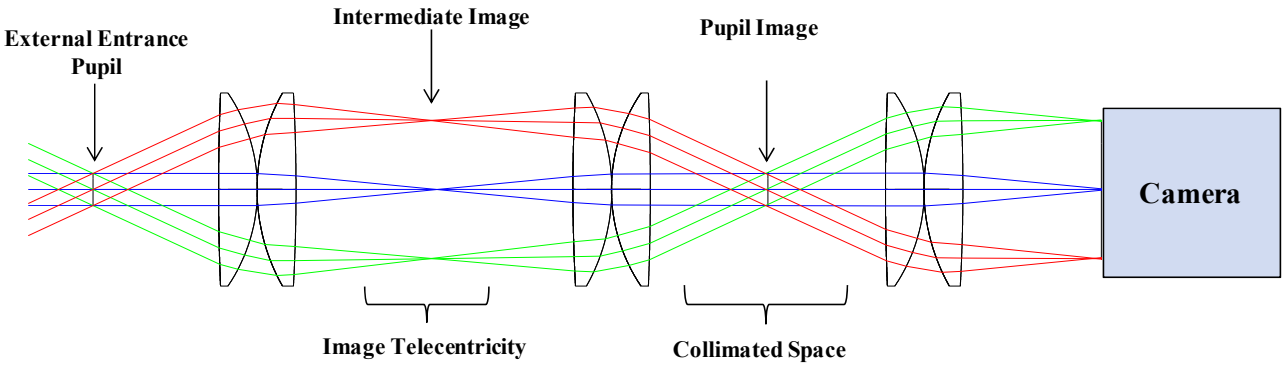

Figure 2. A flexible optical layout for pupil and image plane coding.

When considering the aforementioned design trades for ACIS and the goal to develop a low-cost solution, we converged on developing two testbeds. The first would address target oversampling via sub-pixel coded modulation at the image plane otherwise known as implementing high-resolution programmable pixels or pixel oversampling. In addition, the testbed is coupled to an MIT LL focal plane array with non-uniform pixel sampling. The second testbed addresses the ACIS goal of simultaneous space-time coding at the image plane using a different MITLL focal plane array technology

combined with dynamic pupil encoding. The next section will focus on the coded-aperture programmable pixel imaging (CAPPI) testbed.

3. CODED-APERTURE PROGRAMMABLE PIXEL IMAGING TESTBED

We developed the coded-aperture programmable pixel imaging (CAPPI) testbed to conduct experiments exploring non-uniform pixel sampling and coded-aperture pixel encoding for spatial super-resolution. We also interfaced a re-purposed MIT LL OTCCD as a computational imaging array (CIA), to the testbed for spatial super-resolution experiments. Scaling down from the full capabilities of the testbed described in Section 2 by removing the pupil coding capabilities allowed the object-plane coding testbed to be built using only low-cost COTS optical components. A requirement for the testbed was to sample object data by factors greater than 4×4 over an array of pixels. Image distortion and magnification were important for reconstruction of the image after sampling by the test camera. Illumination uniformity was also an important characteristic influencing the signal-to-noise ratio (SNR) of the data, and so efforts were made in the optical design to limit the variation of image irradiance across the FOV. In this section, we describe how testbed requirements influenced optical component selection.

We used a DMD for dynamic object encoding. Previous work shows that using DMDs for object encoding via structured illumination have the best balance of fill factor, speed, linearity and efficiency in comparison to other spatial light modulator technologies[33]. This approach has advantages in a laboratory setting where ambient lighting can be controlled and object illumination can be optimized for a fixed focal distance. When imaging an object with a known finite range the optical system is less complicated when using the DMD to produce structured illumination rather than using it for encoding an intermediate image plane. Testbeds developed using the latter method include the seminal Rice single-pixel Camera and subsequent work investigating its optical calibration[8,10-11, 34]. By imaging the object onto the DMD directly, stricter requirements are placed on the objective and relay lenses including restricted F/#s and the degree of telecentricity at the intermediate image. Additionally, correction of the Scheimpflug condition for tilted conjugate planes requires the DMD and imaging cameras to be tilted with respect to the optical axis of the relay lens. This introduces keystone distortion causing registration errors between the DMD encoding pattern and the sampling of the focal plane array, which must be accounted for in the data reconstruction. In the CAPPI testbed, the burden of satisfying the Scheimpflug condition is shifted to an illumination path wherein a condenser lens projects a light source toward the DMD with less stringent image quality requirements. Then, by using a transparent chrome on glass USAF 1951 target, the projection and imaging lenses may be used in an inline configuration that simplifies their alignment, removes keystone distortion, and allows for greater flexibility in the selection of COTS components. An illustration of these methods is shown in Figure 3.

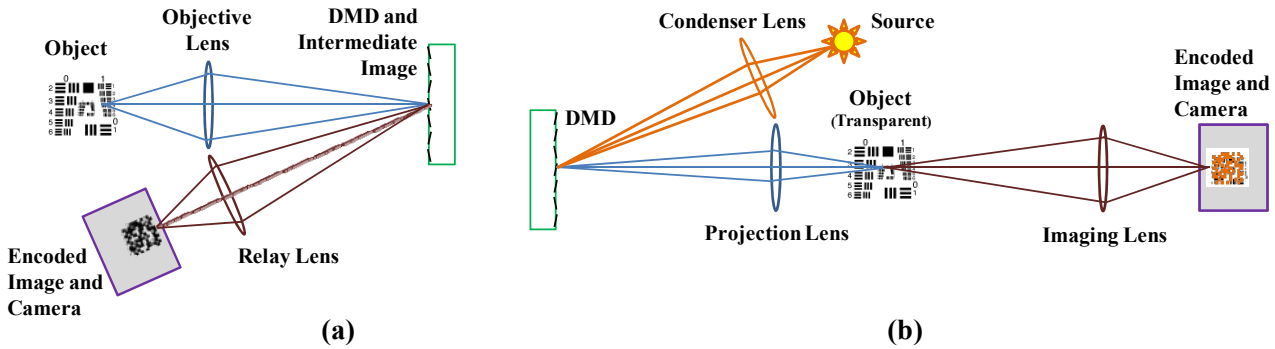

Figure 3. A comparison of object coding methodologies. (a) Object coding at an intermediate image plane and (b) CAPPI object coding via structured illumination.

Component specifications were derived to support system-level requirements for illumination, resolution, and pixel oversampling. Considerations include: 1) pupil matching between the condenser, projection, and imaging lenses, 2) illumination angle restrictions introduced by the DMD, 3) satisfying the Scheimpflug condition, and 4) the relationships between optical resolution, pixel resolution, and magnification. The following paragraphs describe the specific design details related to each of the optical subsystems.

3.1 Illumination Subsystem

The illumination system was designed to provide uniform illumination over the DMD, support high contrast light modulation, and couple light (relatively) efficiently into the projection lens. The DMD selected was a Texas Instruments DLP9500 with a 1920× 1080 array and 10.8 μm micro-mirrors that pivot ± 12° about the plane of the array. Texas Instruments provides an excellent reference for designing DLP-based optical systems[35], and the challenge was to do this using COTS components. The pivot angle on the DMD elements introduces two requirements: 1) the F/# of the condenser lens must be no faster than F/2.4 to separate the input and output ray paths and 2) in order to use the DMD perpendicular to the optical axis of the projection lens, a 24° fold angle must be accommodated in the condenser lens.

A telecentric optical design produces the most uniform black levels for elements in the off position across the entire DMD. This was satisfied with a telecentric Abbe Illumination design which produced a long working distance able to accommodate the projection optics without the use of an expensive TIR prism pair. The condenser lens was a 55 mm focal length commercially available telecentric lens (Edmund Optics 52-271) used at a 2× magnification. At its maximum aperture, it produced a working F/# of F/5.6 at the DMD. In an Abbe design, the light source is imaged directly onto the DMD, which requires homogenization of the light source to remove unwanted structure in the image.

The light source selected for the test bed was a halogen lamp fed into a fiber light guide bundle. A 10 mm hexagonal integrating rod (or light pipe) was used to homogenize its output and (when magnified) produce a 20 mm hexagonal image nearly filling the DMD. Internal reflections within the integration rod create an array of virtual images of the source. The number of virtual images and their relative brightness depends on the NA of the source and the rod geometry. The lateral spacing between the virtual images is equal to the width of the rod. A source that is smaller than the aperture of the rod will produce uniform spatial illumination at the exit surface of the rod, provided that the source NA is appropriately matched to the rod geometry to create a sufficient number of virtual images for homogenization of the output. However, when the source is smaller than the rod width, different sub-aperture regions of the rod's exit surface are illuminated by a discrete angular spectrum corresponding to the relative positions of the virtual images. A combination of the requirements for condenser lens magnification, working F/# at the DMD, commercially available telecentric lens options, and packaging constraints led to a condition where the outer elements of the source array were partially vignetted by the condenser lenses aperture stop. This caused an apparent loss of illumination uniformity of the rod's exit surface, which translated to the DMD, as shown in a simulation of this effect in Figure 4(a).

Two solutions to improve the illumination uniformity were evaluated. Using a light source that fills (or overfills) the integration rod makes each virtual image of the source the full width of the rod, and therefore the array of images is stitched together to appear as a solid extended source. The exit aperture of the rod is then uniformly illuminated both spatially and angularly, which produces a uniform image at the DMD regardless of vignetting at the projection lens as shown in Figure 4(b). However, testing showed this technique to be inadequate because large spatial non-uniformities in the fiber light guide were not completely homogenized. A second solution was to place a diffuser element at the exit aperture of the rod to angularly homogenize the output beam. The downside of this approach is light loss due to both the transmission of the diffuser and increased scatter at angles beyond the acceptance aperture of the condenser lens. Figure 4(c) shows the same light source as in panel (a), but with an opal diffuser placed at the exit of the rod. The diffuser has 30% transmission efficiency and nearly Lambertion output, which homogenizes the beam at the cost of a ~20× irradiance loss at the DMD. Ultimately, both approaches were combined for the ACIS object plane coding testbed. A 12.7 mm fiber bundle light guide (with significant spatial non-uniformities) was used to overfill a 10 mm hexagonal light pipe and an opal diffuser was placed at the exit aperture to angularly homogenize the output.

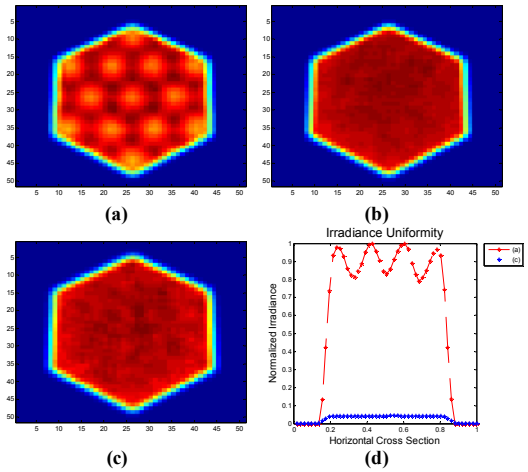

Figure 4. Simulated irradiance at the DMD using different fiber sources. A constant radiance ($W/m^2/sr$) is assumed for all sources: (a) using a 5 mm fiber bundle vignetting is observed at the DMD, (b) with a 12.7 mm fiber bundle the source appears uniform and more light is coupled to the DMD, and (c) uniformity is increased at the expense of throughput by adding a diffuser to the 5 mm fiber bundle. (d) shows horizontal cross sections through plots (a) and (c).

The DMD was aligned normal to the optical axis of the projection lens and illuminated at an incident angle of 24°. A 12° tilt was placed on the integration rod to satisfy the Scheimpflug condition at 2× magnification, which tilts the image plane to focus in the plane of the DMD surface. Mirror elements in the DMD pivot about the diagonal of the array so the illumination system was aligned at a rotation angle of 45° with respect to the plane of the testbed. This placed the DMD array in the same rotational orientation as the imaging cameras, which allows for another important requirement: integer pixel mapping between the DMD and test cameras.

3.2 Projection and Imaging Subsystem

A projection lens is used to image the coded illumination pattern from the DMD to a transparent resolution target, which is then relayed to the test camera with a subsequent imaging lens. Requirements for the projection and imaging subsystems were: 1) to minimize vignetting over the DMD's illuminated area, 2) integer mapping of DMD pixels to the oversampled pixels on the test camera, and 3) to provide sufficient optical resolution to oversample the test camera pixels with DMD illumination patterns.

Matching numerical apertures and pupils is typically important when creating relay systems. NA matching refers to the fact that a single aperture defines the stop of the optical system and thus limits the NA of all the elements in a relay. Pupil matching refers to the ideal condition of matching the exit pupil of one element to the entrance pupil of the following element in a relay. In the case of the CAPPI testbed, pupil and NA matching were only important insofar as light is able to couple through the system without significant vignetting, which would lead to darkened corners in the final image.

Figure 5 shows a raytrace through the testbed at a FOV corresponding to the corner of the DMD. The illumination path is shown in red, and the light that fully passes through the relay to the test camera is shown in black. A lack of NA matching is apparent by observing that light from the DMD (and subsequently from the projection lens) overfills the collection aperture of the following element. However, using a smaller NA for the imaging beam allowed it to wander within the illuminated pupil and provide uniform illumination without the pupils or NAs strictly matched. This allowed for commercially available non-telecentric lenses to be used in the Abbe illumination design. The illumination beam itself is telecentric at the DMD and so the cone of light emerging from the DMD is parallel to the optical axis. This dictated the minimum distance between the DMD and projection lens for light to couple through the system, which placed constraints on the system magnification and selection of a COTS lens designed for the appropriate working distance.

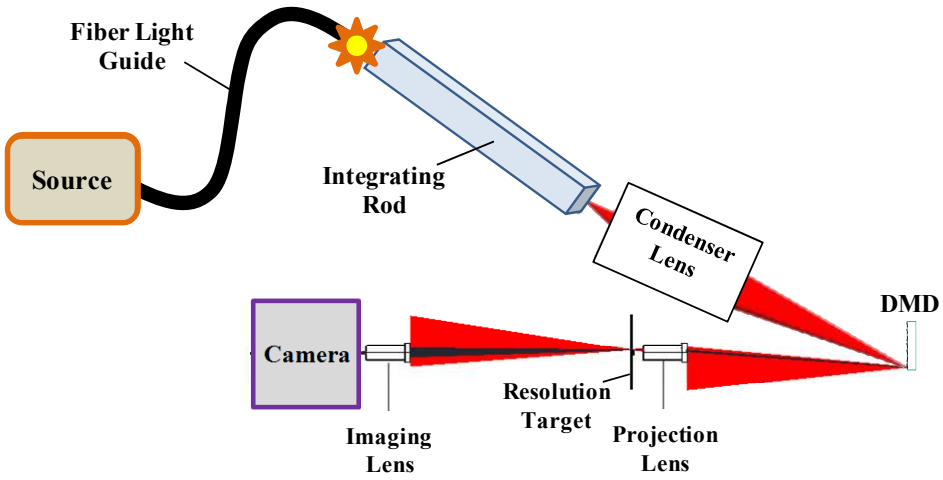

Figure 5. The illumination and imaging ray bundles at the edge of the FOV. The illumination beam (red) is telecentric at the DMD. The lenses are neither pupil nor NA matched as indicated by the clipping of the illumination beam. However, the slow working F/# of the imaging beam (black) allows it to drift within the illumination beam producing uniform image irradiance without strict matching requirements.

CAPPI maps the structured illumination pattern produced by the DMD array to an array of pixels at the test camera. Reconstruction of the image requires knowledge of the mapping between the DMD and test camera arrays. To simplify the reconstruction (i.e. avoid warping the test image with a calibrated distortion table), a distortion requirement was imposed to restrict the image registration error to less than the width of 1 DMD element over the center 1024×1024 elements of the DMD array. This equates to an allowed relative registration error of $[2 \times 512^2]^{-0.5}$ or 0.13% distortion in the lens. Satisfying this stringent distortion requirement with a COTS lens that also met the object distance, magnification, and resolution requirements was somewhat of a challenge, and required analysis of lens prescriptions provided by the manufacturer. An F/2.5 lens with a 25 mm focal length designed for a 150 mm object distance was selected for use as both the projection and imaging lens (Edmund Optics #58-207). Analysis of the encrypted "black box" lens prescriptions provided by the supplier showed that the lens distortion in the testbed configuration was nominally 0.03%, which provided some margin for manufacturing variation.

We imposed integer pixel mapping between the DMD elements to the test camera pixels to minimize image registration issues for improved data recovery. This provided uniform oversampling across the test camera array by eliminating pixel phasing errors. The selected lenses used in series produce a magnification that provided a 36×36 oversampling between the DMD and the OTCCD (i.e. 36×36 DMD pixels map to 1 pixel at the test camera). This selection provided the opportunity to bin DMD pixels to create illumination patterns with multiple oversampling ratios for experimentation: 36×36, 18×18, 12×12, 9×9, 6×6, 4×4, 3×3, and 2×2. Figure 6 illustrates the motivation for selecting a magnification for integer pixel mapping and restricting the distortion of the projection and imaging lenses.

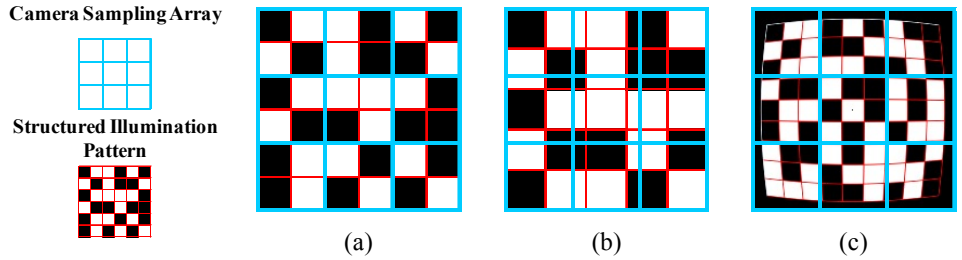

Figure 6. Effects of integer pixel sampling and distortion. (a) 2× 2 pixel oversampling of the structured illumination pattern, (b) a non-integer 1.666× 1.666 oversampling causes a phase shift between the illumination pattern and the test camera array, (c) image distortion changes the oversampling ratio as function of image height.

A baseline camera with smaller pixels (i.e., 2.5 µm) is used to observe the structured illumination pattern at a higher resolution and provide ground truth for the test camera. Integer pixel mapping between the witness camera and the test camera allows for the witness camera pixels to be binned in order to simulate the test camera. A witness camera with 2.5 µm pixels was selected to provide a resolution exactly 6× higher than the 15 µm OTCCD test camera at the same magnification. The magnification of the test and witness cameras was set by observing a binned checkerboard pattern on the DMD and fine-tuning the focus and conjugate distances until a 600× 600 block of pixels at the DMD imaged to 10 × 10 pixels at the witness camera (6× oversampling), and a 720× 720 block of pixels at the DMD imaged to 20× 20 pixels at the test camera (36× oversampling).

Optical resolution is a key aspect of the testbed design. Although the DMD pixels are magnified to the test camera with a 36× 36 pixel oversampling, in practice the maximum useful oversampling ratio is limited by the point spread function of the projection and imaging lenses. The MTF of these lenses was measured and applied to a simulation of its impact on contrast and resolution on the structured illumination pattern at the intermediate image plane, which is depicted in Figure 7(a-i). MTF measurements were conducted using the super-resolved slanted edge technique described in ISO 12233, and performed with commercially available test software[36]. The lens MTF at the Nyquist frequency of the test camera (33 cycles/mm) was measured to be 84%, which qualitatively implies that the resolution of a raw image captured by the OTCCD is limited by the pixel sampling and not the optical point spread function. Contrast degrades for higher spatial frequency mask patterns, which produces a practical limit for oversampling of 6× 6 beyond which the structured illumination pattern approaches a washed out grey image. Replacement of the testbed optics with higher resolution lenses will allow for higher oversampling ratios. We are considering this hardware modification for the next-generation CAPPI testbed.

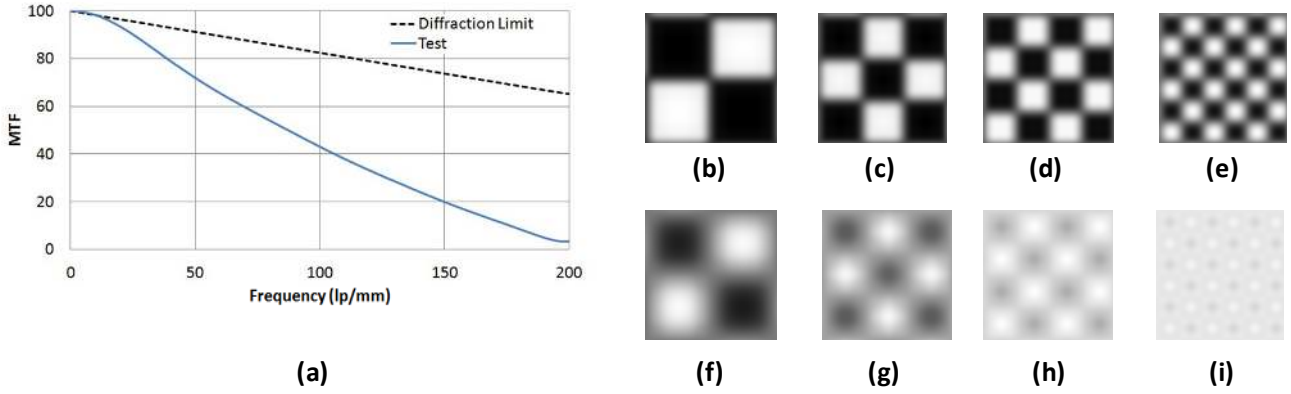

Figure 7. (a) F/2.5, EFL 25 mm projection lens MTF using the ISO 12233 method. The black dashed-line represent contrast and spatial frequencies of interest for an image-based encoding simulation. Diffraction imaging performance at contrast ratios indicated in (a) are shown in (b) with 2× 2, (c) 3× 3, (d), 4× 4, and (e) 6× 6 oversampling. Testbed imaging performance is similarly shown in (f-i).

As a motivation for using the CAPPI testbed as an array-based super-resolution testbed, we have simulated pixel 4×4 oversampling with time-varying, pseudo-random, and binary-valued aperture-codes. Note that we have implemented and explored other aperture codes – Toeplitz, S-matrix, modified uniformly redundant arrays, and others. These implementations are not within the scope of this paper and are deferred to a secondary publication. Figure 8 shows the benefits associated with pixel oversampling as a function of number of masks implemented to generate a high-resolution image (Figure 8(e)). An aberrated point spread function corresponding to the mask contrast of Figure 7(h) is used in the simulation.

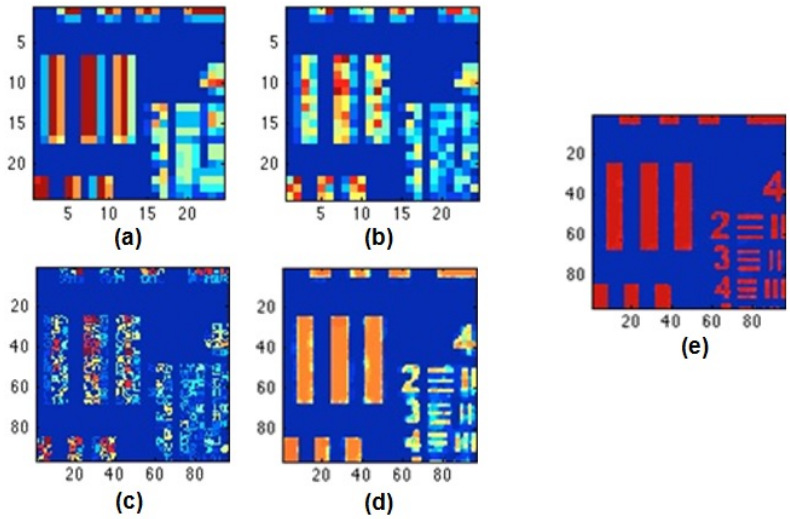

Figure 8. Simulated testbed imaging performance on image reconstruction using pseudo-random and binary modulation with a pixel oversampling rate of 4×4. (a) Low-resolution conventional 24×24 detector measurement. (b) CAPPI single pseudo-random and downsampled projection. Compressive sensing reconstruction estimate of a high-resolution (96×96) target image using a (c) single mask, (d) 10 masks, and (e) 100 masks for 2D high-resolution target recovery in a high signal-to-noise ratio scenario.

We have collected first-light imagery with the CAPPI testbed shown in Figure 9. Initial data collects are focused on exploiting characteristics of the OTCCD including non-uniform pixel phase structure to inform future focal plane development. We have also collected imagery associated with array-based spatial super resolution experiments (similar to the Rice single pixel camera, but using an array) to validate the compressive sensing simulation shown in Figure 8. Testbed imagery will be discussed in a secondary article.

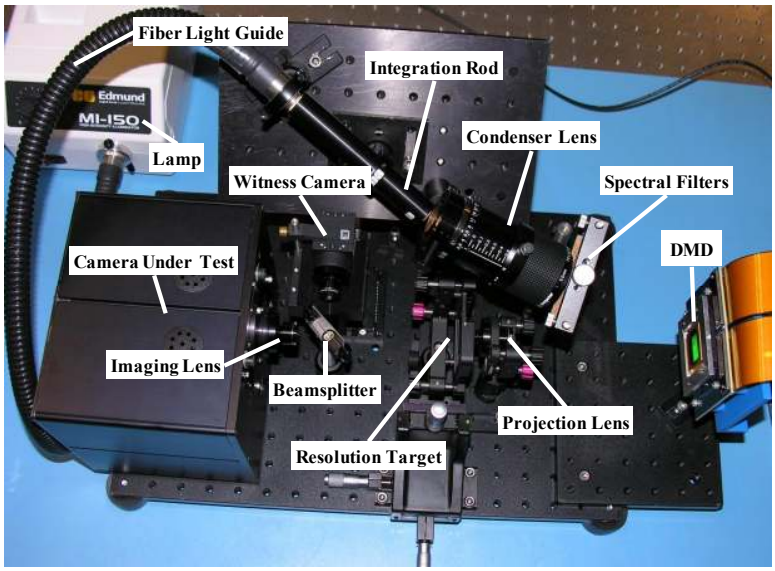

Figure 9. Coded-aperture programmable pixel imaging (CAPPI) testbed for ACIS.

4. SIMULTANEOUS DYNAMIC PUPIL PLANE CODING WITH ON-CHIP PROCESSING

We designed and developed a robust and low-cost simultaneous and dynamic pupil-encoded and time-encoded (PETEI) testbed. Dynamic pupil coding is achieved through the use of a spatial light modulator (SLM), and time-varying and time-synchronized image coding is performed with a DROIC CIAs produced at MIT LL. Together these devices allow the testbed to achieve the capability of the ACIS concept described in Section 2 as a simplified system architecture. Requirements for the PETEI testbed stem from the selection of the SLM, which imposes restrictions on the optical design layout and has consequences on its performance. The use of liquid crystal-based SLMs was ruled out due to polarization and waveband limitations. Two SLM configurations were explored: using a deformable mirror for dynamic wavefront coding and using a DMD for dynamic pupil apodization.

A micro-electro-mechanical (MEMS) deformable mirror with 144 actuators and a 3.5 μm stroke was selected for pupil wavefront encoding experiments (Boston Micromachines Corporation DM140-35-Ux01). The mirror deformation provides a mechanism to encode up to 7 μm of optical path difference into the pupil, which can take the form of low order defocus and tilt terms, or higher order superpositions of the first 36 Zernike polynomials. Encoding the pupil with wavefront aberrations using a deformable mirror is relatively straight forward. A calibration step that involves measuring the mirror response to input parameters and computing the residual error should be preformed to improve image reconstruction accuracy. This can be accomplished by measuring the deformable mirror with an interferometer in a test configuration, provided that the interferometer has sufficient resolution to measure the high order Zernike terms over the aperture of the deformable mirror. We are undergoing complete characterization of SLMs utilized with the PETEI testbed.

Using a DMD for amplitude coding in the pupil poses a few challenges, because DMDs are designed to provide spatial light modulation at a field position (object or image). The DMD array itself acts as a 2 dimensional blazed diffraction grating[37]. Because the micromirror elements pivot about their diagonal, the effective grating pitch is equal to half the pixel diagonal, and the blaze angle is equal to the pivot angle itself. In broadband applications, the resulting point spread function is separated into a spectrum, and multiple diffraction orders will be seen in the image. When designing optics with a diffraction grating a Littrow mounting configuration is often used for high diffraction efficiency and for compact optical designs because diffracted light is directed back in the direction of the incident beam. For maximum efficiency at the Littrow condition, the DMD should be oriented such that the micromirror facets are normal to the incident light when in their ‘on’ position (i.e. for the Texas Instruments DLP9500 described in Section 3 the body of the DMD is tilted at an angle of 12° with respect to the incident beam). The wavelengths of peak efficiency as a function of diffraction order can then be computed from:

$$\lambda_m = \frac{2d \sin \alpha}{m},$$

where d is the grating pitch (7.64 μm for a 10.8 μm DMD element), α is the incident angle (12°), and m is the diffraction order. The efficiency peaks for the first five diffraction orders are then:

Table 1. Efficiency peaks and waveband for diffraction orders in a Littrow mounting condition of TI DLP9500.

Order	Peak Efficiency Wavelength (μm)	Approximate Waveband for Efficiency > 50% (μm)	
1	3.176	2.117	5.716
2	1.588	1.059	2.858
3	1.059	0.706	1.905
4	0.794	0.529	1.429
5	0.635	0.423	1.143

For monochromatic imaging experiments, the efficiency peaks and bandwidths shown in Table 1 indicate that a Littrow mounting configuration will provide good diffraction efficiency for the common laser wavelengths 1.550 and 1.064 μm in the short-wave infrared (SWIR), and 0.633 nm in the visible. The magnitude of the 12° degree blaze angle on the TI DLP9500 is large enough to introduce diattenuation of the reflected beam including strong anomalies at low diffraction orders, but in the 3rd or higher order these polarization effects are less significant[38].

A driving factor of the optical performance is the position at which the SLM is mounted. For uniform encoding across the FOV, the SLM must either define the system aperture stop or be placed at an accessible pupil location. When constructing a testbed from commercially available lenses this typically requires shifting the aperture stop away from its original design location, and may require reducing its diameter to control vignetting. This changes the aberration content of the lens, and potentially its F/# and FOV. The magnitude by which stop shifting changes the aberrations depends on details of the specific lens prescription, which is not generally provided by the manufacturer. As an example, prescriptions of 25 mm and 50 mm commercially available SWIR lenses were obtained and the effects of stop shifting to accommodate the SLM were investigated. To first order, the shorter focal length lens should produce a larger FOV for a fixed detector size, and also have a smaller PSF by way of the faster F/# it achieves when the relatively small deformable mirror (4.4 × 4.4 mm) is used as the aperture stop. However, after analyzing the effects of shifting the aperture stop 35 mm in front of the lenses it was discovered that the shorter focal length lens suffered a much more significant increase in aberrations and a smaller FOV due to vignetting. Results of the analysis are shown in Figure 10. We emphasize that the analysis does not generally apply to all 25 and 50 mm lenses, rather it is intended to emphasize the importance of understanding the lens prescription when using COTS lenses in a configurations for which they were not designed.

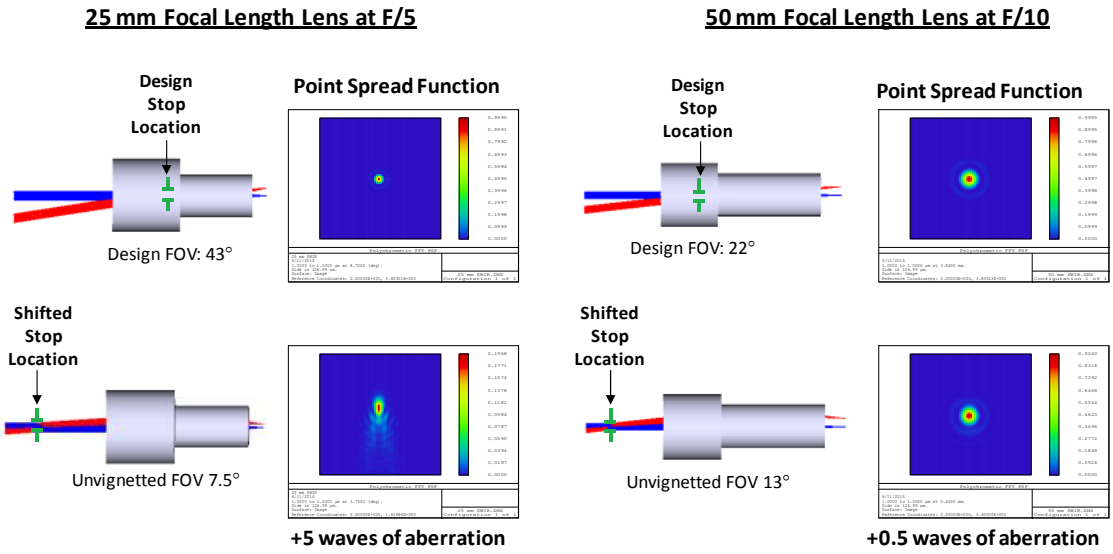

Figure 10. Effects of shifting the aperture stop 35 mm in front of commercially available SWIR lenses. (a) a 25 mm lens, and (b) a 50 mm lens. A 4.4 mm pupil diameter is modeled for both lenses representing the active area of the deformable mirror. Point spread function and wavefront analysis was conducted at the edge of the FOV for a wavelength of 1 μm.

The selected optical layout for the pupil plane coding testbed uses a 50 mm focal length lens with the aperture stop shifted 35 mm in front of the lens. This stop shift provides the working distance sufficient to accommodate a beamsplitter, which allows for both types of spatial light modulators to be used. The deformable mirror is used at normal incidence and the DMD is used in a Littrow configuration. The testbed layout is shown in Figure 11.

We have described and developed the experimental testbed for PETEI in this section. The initial testbed alignment is shown in Figure 12 First-light imagery and testbed validation will be discussed in a subsequent work.

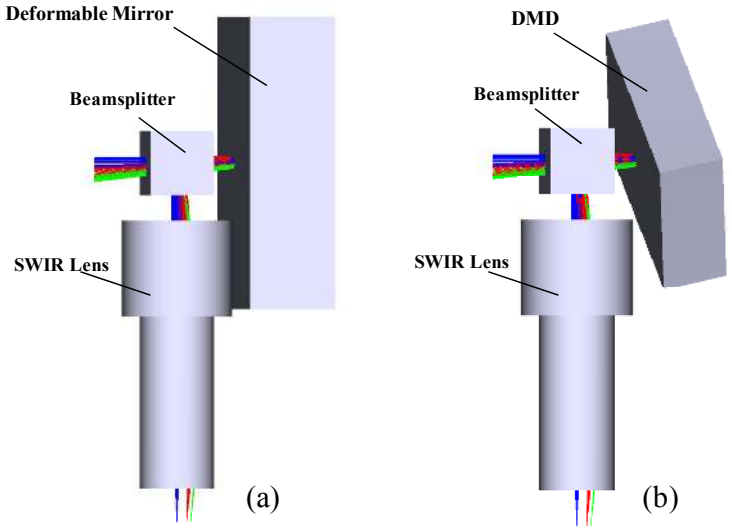

Figure 11. Pupil encoding testbed layout. (a) Phase encoding with a deformable mirror and (b) amplitude coding with a DMD used at the Littrow diffraction angle.

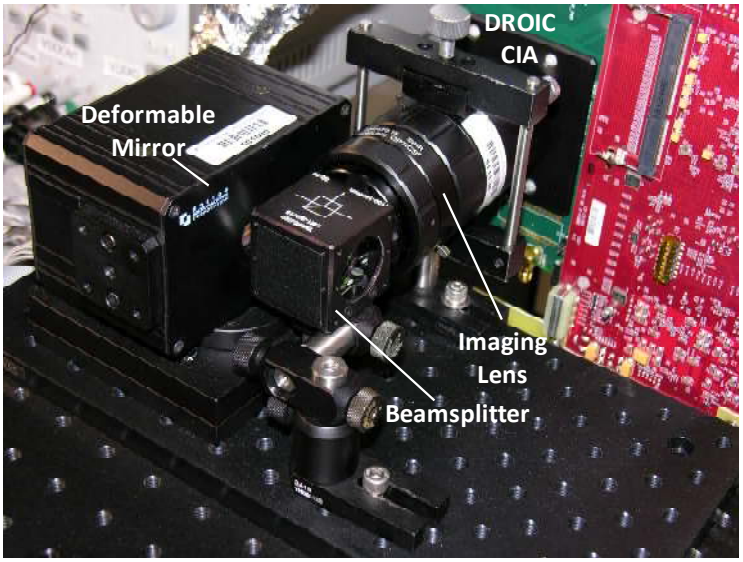

Figure 12. Simultaneous and dynamic pupil-encoded and time-encoded imaging (PETEI) testbed for ACIS.

5. CONCLUSION

We have described the development of two testbeds – CAPPI and PETEI – for research in advanced computational imaging systems. These testbeds enable pixel oversampling and reconfiguration for experiments in spatial super-resolution. Also, the testbeds facilitate simultaneous encoding at pupil and image planes respectively. Lincoln Laboratory focal plane arrays re-purposed as computational imaging arrays are leveraged and uniquely tested with each of the testbeds. Optical layouts for the testbeds were derived based on experimental requirements and the desire to construct low-cost and robust systems using commercially available test hardware. Further characterization and 'first-light' data with our testbeds is still a work in progress. Through the use of the ACIS object coding and pupil coding testbeds MIT LL intends to explore novel sensing modalities to achieve spatial, temporal and depth super-resolution, as well as passive 3D ranging and increased depth of focus.

REFERENCES

[1] Ashok, A., Baheti, P. K., and Neifeld, M. A., "Compressive imaging system design using task-specific information," Appl. Opt. 47(25), 4457-4471 (2008).
[2] Horstmeyer, R., Athale, R., G. Euliss, "Modified light field architecture for reconfigurable multimode imaging," Proc. SPIE 7468, 746804 (2009).
[3] Cathey, W.T., Dowski, E.R., "New Paradigm for imaging systems," Appl. Opt. 41(29), 6080-6092 (2002).
[4] Greengard, A., Schechner, Y., Piestun, R., "Depth from diffracted rotation," Opt. Lett. 21(2), 181-183 (2006).
[5] Wakin, M., et al., "An Architecture for compressive imaging," Proc. of IEEE, 1273-1276 (2006).
[6] Veeraraghavan, A., "Dappled Photography: Mask Enhanced Cameras for Heterodyned Light Fields and Coded Aperture Refocusing," ACM Transactions on Graphics 26(3), (2007).
[7] Arce, G. R., Brady, D.J., Carin, L., Arguello, H., Kittle, D.S., "Compressive coded aperture spectral imaging: An introduction," IEEE Signal Processing Magazine 31(1), 105-115 (2014).
[8] Wakin, M., Laska, J., Duarte, M., Baron, D., Sarvotham, S., Takhar, D., Kelly, K., and Baraniuk, R., "An Architecture for compressive imaging," Proc. of IEEE, 1273-1276 (2006).
[9] Dunlop, M., Jansen, P., and Gehm, M., "Adaptive, Feature-Specific Spectral Imaging Classifier," in Imaging and Applied Optics, OSA Technical Digest Optical Society of America, paper CMD3, (2011).
[10] Takhar, D., Laska, J. N., Wakin, M. B., Duarte, M. F., Baron, D., Sarvotham, S., Kelly, K. F., Baraniuk, R. G., "A New Compressive Imaging Camera Architecture using Optical-Domain Compression," Proc. SPIE 6065, 43-52 (2006).
[11] Duarte, M. F., Davenport, M. A., Takhar, D., Laska, J. N., Sun, T., Kelly, K. F., and Barniuk, R. G., "Single-pixel imaging via compressive sampling," IEEE Signal Process. Mag., 25(2), 83-91 (2008).

[12] Bub, G., Tecza, M. , Helmes, M., Lee, P., and Kohl, P., "Temporal pixel multiplexing for simultaneous high-speed high-resolution imaging," Nature Methods 7(3), 208-211 (2010).
[13] Reddy, D., Veeraraghavan, A., and Chellappa, R., "P2C2:Programmable Pixel Compressive Camera for High Speed Imaging," In CVPR, 329-336 (2011).
[14] Llull, P., Liao,X., Yuan, X., Yang, J., Kittle, D., Carin, L., Sapiro, G., and Brady, D., "Coded aperture compressive temporal imaging," Opt. Express 21, 10526-10545 (2013).
[15] Ben-Esra, M., Zomet, A., and Nayar, S.K., "Video super-resolution using controlled subpixel detector shifts," IEEE Transactions on Pattern Analysis and Machine Intelligence 27, 97-987 (2005).
[16] Raskar, R., Agrawal, A., and Tumblin, J., "Coded exposure photography: motion deblurring using fluttered shutter," Proc. IEEE Computer Society Conference Computer Vision Pattern Recognition, 1-8 (2007).
[17] Llull, P., Yuan, X., Liao, X., Yang, J., Carin, L., Sapiro, G., and Brady, D., "Compressive extended depth of field using image space coding," in Classical Optics, OSA Technical Digest, (2014).
[18] Fernandez-Cull, C., Bolstad, A. and Tyrrell, B. M., "On-chip temporal multiplexing with a digital focal plane array," SPIE DSS, (2013).
[19] Fernandez-Cull, C., Tyrrell, B. M., D'Onofrio, R., Bolstad, A., Lin, J., Little, J. W., Blackwell, M., Renzi, M., and Kelly, M., "Smart pixel imaging with computational-imaging arrays," Proc. of SPIE 9070, 90703D (2014).
[20] Little, J. W., Tyrrell, B. M., D'Onofrio, R., Berger, P. J., Fernandez-Cull, C., "Digital pixel CMOS focal plane array with on-chip multiply accumulate units for low-latency image processing," Proc. SPIE 9070, 90703B (2014).
[21] Fernandez-Cull, C., Shepard, R., Tyrrell, B. M., and D'Onofrio, R., "Simultaneous Dynamic Pupil Coding with On-chip Coded Aperture Temporal Imaging," in Imaging and Applied Optics, OSA Technical Digest, (2014).
[22] Shi, B., Zhao, H., Ben-Ezra, M., Yeung, S.-K., Fernandez-Cull, C., Shepard, R.H., Barsi, C., and Raskar, R., "Sub-Pixel Layout for Super-Resolution with Images in an Octic Group," In Proc. European Conf. on Computer Vision (ECCV), (2014).
[23] Burke, B. E., Reich, R.K., Savoye, E.D., Tonry, J.L, "An orthogonal-transfer CCD imager," IEEE J. Electron Devices 41(12), 2482-2484 (1994).
[24] Tonry, J., and Burke, B. E., "The Orthogonal Transfer CCD," Experimental Astronomy 8, 77-87 (1998).
[25] Kelly, M., Berger, R., Colonero, C., Gregg, M., Model, J., Mooney, D., Ringdahl, E., "Design and testing of an all-digital readout circuit for infrared focal plane arrays," Proc. SPIE. 5902, 105-115 (2005).
[26] Tyrrell, B. M., Anderson, K., Baker, J., Berger, R., Brown, M., Colonero, C., Costa, J., Holford, B., Kelly, M., Ringdahl, E., Schultz, K., and Wey, J., "Time Delay Integration and In-Pixel Spatiotemporal Filtering Using a Nanoscale Digital CMOS Focal Plane Readout," IEEE Transactions on Electron Devices, 56(11), 2516-2523 (2009).
[27] Kelly, M.W. and Blackwell, M.H., "ADVANCES IN DETECTORS: Digital-pixel FPAs enhance infrared imaging capabilities," Laser Focus World, (2013).
[28] Ashok, A., and Neifeld, M., "Pseudorandom phase masks for superresolution imaging from subpixel shifting," Appl. Opt. 46(12), 2256-2268 (2007).
[29] Quirin, S., Peterka, D. S., and Yuste, R., "Instantaneous three-dimensional sensing using spatial light modulator illumination with extended depth of field imaging," Opt. Exp. 21, (2013).
[30] Cheng, A., Goncalves, J. T., Golshani, P., Arisaka, K., and Portera-Cailliau, C., "Simultaneous two-photon calcium imaging at different depths with spatiotemporal multiplexing," Nat. Methods 8, 139-142 (2011).
[31] Piro, N., Pengo, T., Oliver, N., and Manley, S., "Improved 3D Superresolution Localization Microscopy Using Adaptive Optics," (2014).
[32] Sasián, J., "Introduction to Aberrations in Optical Imaging Systems," Cambridge University Press, 24-25, (2013).
[33] Frankowski, G., and Hainich, R., "DLP-Based 3D Metrology by Structured light or Projected Fringe Technology for Life Sciences and Industrial Metrology," Proc. of SPIE 7210, 72100C-1 (2009)
[34] Wu, Y., Chen, C., Ye, P., Wang, Z., Arce, G. R., and Prather, D. W., "Optical Calibration of a Digital Micromirror Device (DMD)-based Compressive Imaging (CI) System", Proc. of SPIE 7210, 72100F-1 (2009).
[35] Texas Instruments, "DLP System Optics", Application Report DLPA022, (2010)
[36] Kurtsev, o. "QuickMTF 2.06," (2013)
[37] Rice, J. P., et al., "DMD diffraction measurements to support design of projectors for test and evaluation of multispectral and hyperspectral imaging sensors," Proc. of SPIE 7210, 72100D (2009)
[38] Palmer, C., "Diffraction Grating Handbook," Richardson Grating Laboratory, 5th Edition, Chapter 9, (2002)